Available online at www.sciencedirect.com
ScienceDirect
Journal of Sound and Vibration 300 (2007) 394–413
JOURNAL OF SOUND AND VIBRATION
www.elsevier.com/locate/jsvi

Short Communication

Experimental validation of a finite-element model updating procedure

S. Kanev[a,*], F. Weber[b], M. Verhaegen[a]

[a]*Delft University of Technology, Delft Center for Systems and Control, Mekelweg 2, 2628 CD Delft, The Netherlands*
[b]*Structural Engineering Research Laboratory, Swiss Federal Laboratories for Materials Testing and Research, Ueberlandstrasse 129, CH-8600 Duebendorf, Switzerland*

Received 25 October 2004; received in revised form 22 March 2006; accepted 30 May 2006
Available online 13 November 2006

Abstract

This paper validates an approach to damage detection and localization based on finite-element model updating (FEMU). The approach has the advantage over other existing methods to FEMU that it simultaneously updates all three finite-element model matrices at the same time preserving their structure (connectivity), symmetry and positive-definiteness. The approach is tested in this paper on an experimental setup consisting of a steel cable, where local mass changes and global change in the tension of the cable are introduced. The new algorithm is applied to identify the size and location of different changes in the structural parameters (mass, stiffness and damping). The obtained results clearly indicate that even small structural changes can be detected and localized with the new method. Additionally, a comparison with many other FEMU-based methods has been performed to show the superiority of the considered method.

1. Introduction

Finite-element model updating (FEMU) [1–3] is a data-driven approach to the problem of detecting and localizing damages in industrial structures. Although, numerous publications have appeared recently in the literature [4–17], most of the existing methods are unable to simultaneously update all of the finite element model (FEM) matrices and at the same time keeping their structural properties, such as connectivity (sparsity/structure), symmetry and positive-definiteness. As pointed out in Ref. [1], the FEMU problem has not yet been solved satisfactorily and further research is still needed.

A well-known difficulty in trying to update all FEM matrices from vibration data is the non-uniqueness of solution. This difficulty is usually circumvented by updating one (or at most two) of the FEM matrices so that it is as closely as possible to the corresponding nominal one [4,13,7,14,1]. The usual equality constraints, added to this cost function, are the mass-orthogonality of the mode shapes, the quadratic eigenvalue equation and symmetry. The main advantage of the so-defined FEMU problem is that, using the Lagrange multiplier

*Corresponding author. Tel.: +31 15 27 86707; fax: +31 15 27 86679.
E-mail addresses: S.Kanev@DCSC.TUDelft.NL (S. Kanev), felix.weber@empa.ch (F. Weber), M.Verhaegen@DCSC.TUDelft.NL (M. Verhaegen).

0022-460X/$ - see front matter © 2006 Published by Elsevier Ltd.
doi:10.1016/j.jsv.2006.05.043

technique, one can derive an analytic solution to the problem. Shortcoming is that there is no guarantee that the updated matrix will be positive-definite. Moreover, such updating destroys the connectivity of the updated matrix.

In an attempt to deal with the problem of preserving the sparsity in the updated stiffness matrix **K**, Smith [14] includes a sparsity constraint into the problem that resulted in an iterative optimization problem. The alternating projection method is subsequently used to solve the problem. A similar idea is pursued by Abdalla in Ref. [10], where additional attention is paid to the fact that the modal parameters are in practice inaccurate and therefore the standard equality constraints maybe inconsistent. To deal with that problem the stiffness matrix **K** is updated in such a way that it is symmetric positive-definite, it shares the same structure as the nominal matrix $\mathbf{K}_N$ and makes the norm of the eigenvalue equation as small as possible. Again, the resulting optimization problem is solved using the alternating projection method that has a rather slow convergence.

The problem considered in this paper is even more general: it is aimed to update *all three* FEM matrices simultaneously such that they (a) remain symmetric and positive semi-definite, (b) share the same sparsity as the nominal matrices, and (c) try to match the current modal data as closely as possible (in the sense of norm, defined later in the paper). In order to make sure that the resulting solution is unique it is assumed that one, or at most a few, non-zero elements of one of the FEM matrices are known or remain constant. In a real-life structure these can, for instance, correspond to nodes with increased reliability where the chance of structural damage is reduced. In cases that no a priori information is present about which elements to consider as fixed, an additional term can be added to the cost function that punishes the deviations from the nominal values, which makes the optimal solution unique. Clearly, this approach is much less restrictive than the standard assumption that one of the matrices is completely known.

An approach to solve the above general problem formulation was recently proposed in Ref. [18]. In the present paper this method is experimentally validated on a test setup consisting of a steel cable located at EMPA, Switzerland. The cable is excited by a shaker and several accelerometers are used to measure the vibrations. The considered test scenarios consist of attaching additional mass elements at certain locations of the cable, which cause changes in some entries of the mass matrix, as well as changing the tension of the cable which, in turn, changes the stiffness matrix. These changes are then to be identified by the proposed algorithm. It will be demonstrated that the new method is indeed capable of accurately detecting and localizing the increased mass even though only one entry of the mass matrix is assumed as constant, namely the first entry on the main diagonal. To highlight the performance of the method, it is compared to a number of other existing methods. The results of this comparison clearly highlight the outstanding performance of the approach proposed in this paper.

The paper is structured as follows. In Section 2, the experimental setup is explained and FEM of the cable is summarized. Section 3 contains the problem formulation and a brief explanation of the FEMU method used. The experimental results are reported and discussed in Section 4, where the new method is applied to the problem of identifying the locations and sizes of changed structural parameters (mass, stiffness and damping). For comparison, many other existing methods have also been implemented and tested on the same data and it is demonstrated that the new approach outperforms the others. After the acknowledgements in Section 6, the paper is concluded with some final remarks in Section 5.

2. Application

2.1. System description

The structure under consideration is a 15.50 m long steel wire strand that is tensioned with 33.3 kN. The setup is schematically visualized in Fig. 1. The cable is excited by an electro-dynamically driven shaker positioned at 14.34 m, depicted on Fig. 2 (left). The shaker force is measured by three force transducers whose sum is the measured excitation force, see Fig. 2 (right). The input signal of the shaker is a sweep function that excites the cable for 300 s starting at 0.5 Hz and stopping at 22 Hz. In this way, the first eight cable modes are excited as can be seen from the power spectral density estimate in Fig. 3. Nine accelerometers are used as sensors. Their locations throughout the cable, together with some other cable parameters, are given in Table 1.

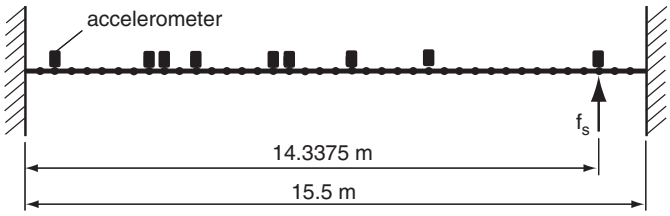

Fig. 1. Scheme of the test cable.

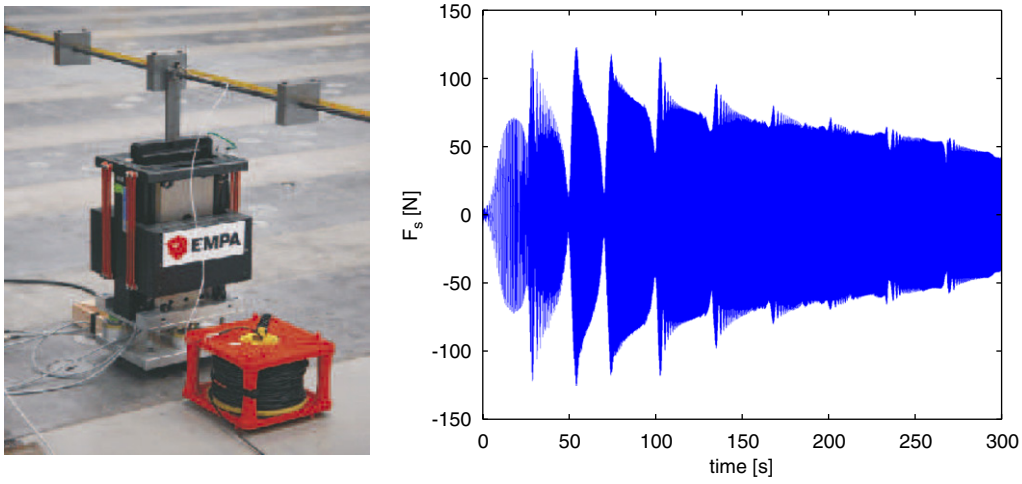

Fig. 2. Left: Shaker connected to 15.50 m long steel wire strand. Right: Measured shaker force during sweep excitation.

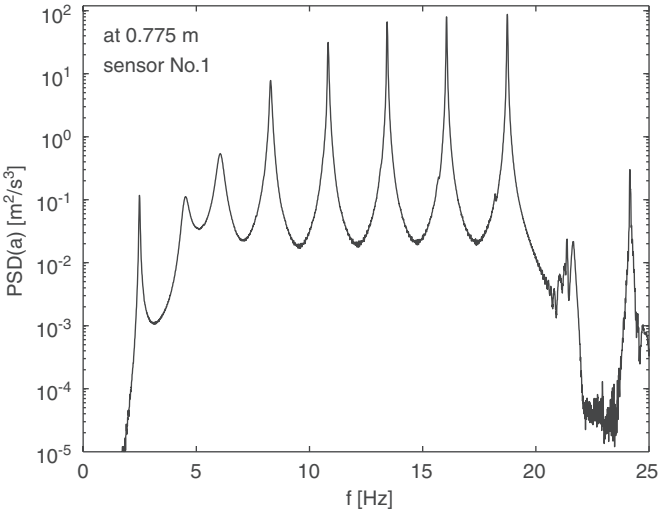

Fig. 3. Measured power spectral density estimate of acceleration at 0.775 m.

2.2. Test cases

There are three sets of test scenarios used to validate the FEMU method considered in this paper.

2.2.1. Local mass changes

Additional weights are attached to the cable in order to change the nominal cable parameters. The nominal cable weight per unit length is 6.03 kg/m, see Table 1. The weight of the structure is changed by adding either

Table 1
Cable parameters and sensor locations

Parameter	Variable	Value
Cable length (m)	l	15.5
Shaker position (m)	p_s	14.3374
Cable weight per unit length (kg/m)	δl	6.0377
Cable tension (N)	T	33.3×10^3
Position of sensor no. 1 (m)	—	0.775
Position of sensor no. 2 (m)	—	3.1
Position of sensor no. 3 (m)	—	3.4875
Position of sensor no. 4 (m)	—	4.2625
Position of sensor no. 5 (m)	—	6.2
Position of sensor no. 6 (m)	—	6.5875
Position of sensor no. 7 (m)	—	8.1375
Position of sensor no. 8 (m)	—	10.075
Position of sensor no. 9 (m)	—	14.3375

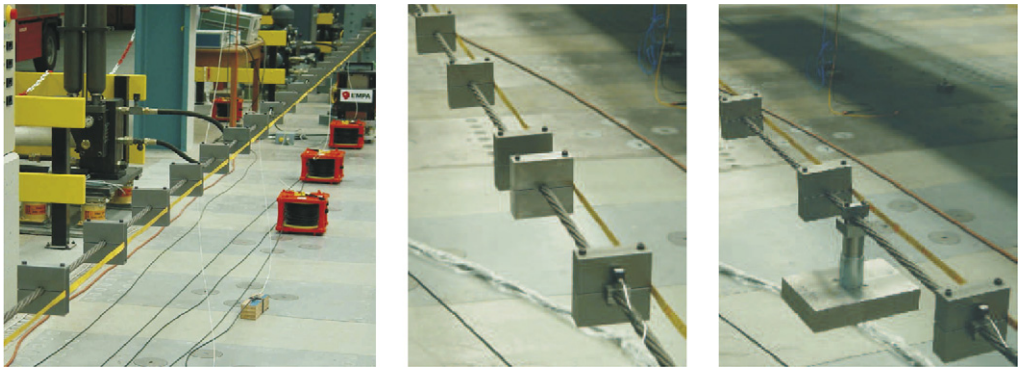

Fig. 4. Left: Nominal cable with no additional masses. Middle: Additional small mass. Right: Additional big mass.

a small mass (2.517 kg) or a big mass (12.840 kg) at an arbitrary location as depicted on Fig. 4. Experiments are made with these masses attached to the cable at two different positions, see Table 2. These experimental test scenarios are used to validate the new method and to compare it to a number of existing FEMU methods, namely those listed in Table 5.

2.2.2. *Local mass and global stiffness change*

This set of test scenarios consist of two experiments: one nominal, and another one in which two changes have been introduced, namely an increased local mass at node 19 and an increased cable tension. Table 3 summarizes these two test scenarios.

2.2.3. *Local changes in mass, stiffness and damping*

The experimental setup does not make it possible to introduce simultaneously local changes in mass, damping and stiffness at specific nodes. For that reason, an additional test scenario has been generated in simulation in order to test the performance of the method in the most general case of changes in all three FEM matrices (Table 4). Although this test scenario is rather idealistic since the modal parameters are exactly known at all degrees of freedom (dof), it is still useful for the purposes of comparison between the novel method and other existing methods under perfect conditions.

Table 2
Test scenarios: mass change

Scenario	Additional mass (kg)	Position (m)	Node in FEM
1	12.84	4.65	12
2	2.517	4.65	12
3	12.84	5.0375	13
4	2.517	5.0375	13

Table 3
Test scenarios: mass and cable tension change

Scenario	Additional mass (kg)	Node	Cable tension (kN)
5	—	—	36.5
6	7.363	19	38.2

Table 4
Simulation test scenario: local changes in mass, damping and stiffness

Scenario	Change m	Node	Change $\mathbf{k}$	Node	Change $\mathbf{c}$	Node
7	+5	12	−10%	13	+0.3	26

2.3. Finite-element model of the cable

For modelling purposes, the cable is divided into 40 pieces of equal length (0.3875 [kg]) resulting in the following FEM:

$$\mathbf{M}_N\ddot{\mathbf{x}}(t) + \mathbf{C}_N\dot{\mathbf{x}}(t) + \mathbf{K}_N\mathbf{x}(t) = \mathbf{B}\mathbf{F}_m(t), \tag{1}$$

where $\mathbf{M}_N = \mathbf{M}_N^{\mathrm{T}} > 0$, $\mathbf{C}_N = \mathbf{C}_N^{\mathrm{T}} \geqslant 0$ and $\mathbf{K}_N = \mathbf{K}_N^{\mathrm{T}} \geqslant 0$ are the mass, damping and stiffness matrices of the cable, $\mathbf{x}(t) \in \mathbb{R}^n$ is the vector of the generalized displacements at the $n = 39$ nodal points, $\mathbf{F}_m(t) \in \mathbb{R}$ is the shaker excitation force, and $\mathbf{B} \in \mathbb{R}^n$ is a vector that represents the location of the shaker at node 37, i.e. all elements are equal to zero except the 37th element, which is equal to one. Let $\mathbf{e}_i$ represent the ith row of the 39×39 identity matrix. Then the measured output signal is given by

$$\mathbf{y}(t) = [\mathbf{e}_2 \ \ \mathbf{e}_8 \ \ \mathbf{e}_9 \ \ \mathbf{e}_{11} \ \ \mathbf{e}_{16} \ \ \mathbf{e}_{17} \ \ \mathbf{e}_{21} \ \ \mathbf{e}_{26} \ \ \mathbf{e}_{37}]^{\mathrm{T}}\ddot{\mathbf{x}}(t). \tag{2}$$

The FEM matrices in Eq. (1) have the following structure:

$$\mathbf{M}_N = \begin{bmatrix} m_{1|2} & m_{2|2} & & & & \\ m_{2|2} & m_{1|2} + m_{1|3} & m_{2|3} & & & \\ & \ddots & \ddots & \ddots & & \\ & & m_{2|n-2} & m_{1|n-2} + m_{1|n-1} & m_{2|n-1} & \\ & & & m_{2|n-1} & m_{1|n-1} & \end{bmatrix}, \tag{3}$$

$$\mathbf{C}_N = \begin{bmatrix} c_{1|2} & c_{2|2} & & & & \\ c_{2|2} & c_{1|2}+c_{1|3} & c_{2|3} & & & \\ & \ddots & \ddots & \ddots & & \\ & & c_{2|n-2} & c_{1|n-2}+c_{1|n-1} & c_{2|n-1} & \\ & & & c_{2|n-1} & c_{1|n-1} & \end{bmatrix}, \tag{4}$$

$$\mathbf{K}_N = \begin{bmatrix} k_{1|2} & k_{2|2} & & & & \\ k_{2|2} & k_{1|2}+k_{1|3} & k_{2|3} & & & \\ & \ddots & \ddots & \ddots & & \\ & & k_{2|n-2} & k_{1|n-2}+k_{1|n-1} & k_{2|n-1} & \\ & & & k_{2|n-1} & k_{1|n-1} & \end{bmatrix}, \tag{5}$$

where nominally

$$m_{1|i} = \frac{1}{3}m\delta l, \quad c_{1|i} = \frac{1}{3}c\delta l, \quad k_{1|i} = \frac{T}{\delta l},$$
$$m_{2|i} = \tfrac{1}{2}m_{1|i}, \quad c_{2|i} = \tfrac{1}{2}c_{1|i}, \quad k_{2|i} = -k_{1|i} \tag{6}$$

for $i = 1, 2, \ldots, n$.

The cable model (3)–(4) is a linear truss element model; for more details on the derivation of such models please consult [19]. The numerical values for the parameters m, T and δl are reported in Table 1; the damping parameter c is not given since it is not measured.

3. The new FEMU approach

3.1. Problem formulation and preliminaries

Consider the FEM (1) representing the nominal, n-dof undamaged structure. Suppose further that, as a result of structural damage, the FEM becomes

$$\mathbf{M}\ddot{\mathbf{x}}(t) + \mathbf{C}\dot{\mathbf{x}}(t) + \mathbf{K}\mathbf{x}(t) = 0, \tag{7}$$

where the structure (often termed *connectivity* in the literature) of the matrices $\{\mathbf{M}, \mathbf{K}, \mathbf{C}\}$ is the same as the nominal matrices $\{\mathbf{M}_N, \mathbf{K}_N, \mathbf{C}_N\}$, given in Eqs. (3)–(5), but the values for one or more of the entries $\{m_{i|q}, k_{i|q}, c_{i|q}\}$ have changed. The goal of the paper is as follows: given the measurements of $\mathbf{y}(t)$, defined in Eq. (2), estimate the entries $\{m_{i|q}, k_{i|q}, c_{i|q}\}$ of the FEM matrices $\{\mathbf{M}, \mathbf{K}, \mathbf{C}\}$. By comparing these estimates to their nominal values one can both detect, localize and quantify damages in the structure.

The approach proposed in this paper uses the measurement data to estimate the modal parameters, which are then used in the process of identification of the structural parameters. Since not all dof are measured, the mode shapes can only be estimated at the dof where the sensors are located. In this paper the missing values of the mode shapes are recovered by means of the so-called B-spline interpolation technique. Furthermore, it is a well-known fact that, in practice, only the modal parameters for the first several modes can be estimated accurately. In this paper all modes are estimated via the state–space model, but only the first five are used for the identification of the structural parameters.

Given the FEM matrices, the modal parameters (i.e. the natural frequencies $\omega_i \in \mathbb{R}$, damping ratios $\xi_i \in \mathbb{R}$, and the mode shapes $\boldsymbol{\phi}_i \in \mathbb{C}^n$, $i = 1, 2, \ldots, n$) can be computed by solving the following:

$$\mathbf{M}\boldsymbol{\phi}_i\lambda_i^2 + \mathbf{C}\boldsymbol{\phi}_i\lambda_i + \mathbf{K}\boldsymbol{\phi}_i = 0, \quad i = 1, 2, \ldots, n, \tag{8}$$

where $\lambda_i \in \mathbb{C}$ are the eigenvalues and $\boldsymbol{\phi}_i$—the eigenvectors (coinciding with the mode shapes of the structure). From the eigenvalues, the natural frequencies and the damping ratios can be computed. Collecting the

eigenvectors and eigenvalues in the matrices

$$\mathbf{\Phi} = [\boldsymbol{\phi}_1 \;\; \boldsymbol{\phi}_2 \;\; \ldots \;\; \boldsymbol{\phi}_n] \in \mathbb{C}^{n\times n},$$

$$\mathbf{\Lambda} = \mathrm{diag}\{[\lambda_1 \;\; \lambda_2 \;\; \ldots \;\; \lambda_n]\} \in \mathbb{C}^{n\times n}, \tag{9}$$

Eq. (8) can be written in a matrix form as the following quadratic eigenvalue problem:

$$\mathbf{M\Phi\Lambda}^2 + \mathbf{C\Phi\Lambda} + \mathbf{K\Phi} = 0. \tag{10}$$

In the case of viscous damping ($\mathbf{C} \neq 0$), the following general orthogonality conditions hold for some vectors $\mathbf{v}_1, \mathbf{v}_2 \in \mathbb{C}^{2n}$ [20]:

$$\mathbf{\Psi}^{\mathrm{T}} \begin{bmatrix} \mathbf{C} & \mathbf{M} \\ \mathbf{M} & 0 \end{bmatrix} \mathbf{\Psi} = \mathrm{diag}\{\mathbf{v}_1\}, \tag{11}$$

$$\mathbf{\Psi}^{\mathrm{T}} \begin{bmatrix} \mathbf{K} & 0 \\ 0 & -\mathbf{M} \end{bmatrix} \mathbf{\Psi} = \mathrm{diag}\{\mathbf{v}_2\}, \tag{12}$$

where $\mathrm{diag}\{\mathbf{v}\}$ denotes a diagonal matrix the vector $\mathbf{v}$ on the main diagonal, and where

$$\mathbf{\Psi} = \begin{bmatrix} \mathbf{\Phi} & \mathbf{\Phi}^* \\ \mathbf{\Phi\Lambda} & \mathbf{\Phi}^*\mathbf{\Lambda}^* \end{bmatrix}. \tag{13}$$

It is easy to show that, when the $\mathbf{C}$ matrix is zero, the general orthogonality conditions (11) and (12) simplify to the following well-known standard conditions

$$\mathbf{\Phi}^{\mathrm{T}}\mathbf{M\Phi} = \mathrm{diag}\{\mathbf{w}_1\},$$

$$\mathbf{\Phi}^{\mathrm{T}}\mathbf{K\Phi} = \mathrm{diag}\{\mathbf{w}_2\}. \tag{14}$$

The mode shapes are sometimes normalized with respect to the mass matrix, although such normalization is not required by the method used in this paper. The vectors $\mathbf{v}_1$ and $\mathbf{v}_2$ are considered here as unknown.

Assume that the first r modes are estimated and represented by the r pairs $\{\hat{\boldsymbol{\phi}}_i, \hat{\lambda}_i\}$, and define the matrices

$$\hat{\mathbf{\Phi}} = [\hat{\boldsymbol{\phi}}_1 \;\; \hat{\boldsymbol{\phi}}_2 \;\; \ldots \;\; \hat{\boldsymbol{\phi}}_r] \in \mathbb{C}^{n\times r}, \quad \hat{\mathbf{\Lambda}} = \begin{bmatrix} \hat{\lambda}_1 & & \\ & \ddots & \\ & & \hat{\lambda}_r \end{bmatrix} \in \mathbb{C}^{r\times r}. \tag{15}$$

Clearly, due to the inaccuracies in these estimated quantities, substituting them, via $\mathbf{\Psi}$, in the orthogonality conditions (11)–(12) will, in general, result in non-diagonal matrices. Similarly, Eq. (10) does not necessarily hold with $\{\mathbf{\Phi}, \mathbf{\Lambda}\}$ replaced by $\{\hat{\mathbf{\Phi}}, \hat{\mathbf{\Lambda}}\}$. Eqs. (10)–(12)) will hold only approximately. Therefore, these are only used in this paper for defining the cost function to be optimized rather than constraints that can turn out to be infeasible.

3.2. Optimization problem

The FEMU approach, originally proposed in Ref. [18], is summarized here. The method is based on an optimization problem in the form of a least-squares with positivity constraints. Such problems can be solved very efficiently.

In defining the cost function, the three conditions (10)–(12) are used. In order to get rid of the unknown vectors $\mathbf{v}_1$ and $\mathbf{v}_2$, and bearing in mind that these equations will hold only approximately for the estimated modal parameters, these are written as follows:

$$\mathbf{M}\hat{\mathbf{\Phi}}\hat{\mathbf{\Lambda}}^2 + \mathbf{C}\hat{\mathbf{\Phi}}\hat{\mathbf{\Lambda}} + \mathbf{K}\hat{\mathbf{\Phi}} \approx 0, \tag{16}$$

$$\hat{\boldsymbol{\psi}}_i^{\mathrm{T}} \begin{bmatrix} \mathbf{C} & \mathbf{M} \\ \mathbf{M} & 0 \end{bmatrix} \hat{\boldsymbol{\psi}}_j \approx 0, \quad \forall i,\ j \neq i, \tag{17}$$

$$\hat{\boldsymbol{\psi}}_i^{\mathrm{T}} \begin{bmatrix} \mathbf{K} & 0 \\ 0 & -\mathbf{M} \end{bmatrix} \hat{\boldsymbol{\psi}}_j \approx 0, \quad \forall i,\ j \neq i, \tag{18}$$

where $\hat{\boldsymbol{\psi}}_i$ is the ith column of the matrix

$$\hat{\boldsymbol{\Psi}} = \begin{bmatrix} \hat{\boldsymbol{\Phi}} & \hat{\boldsymbol{\Phi}}^* \\ \hat{\boldsymbol{\Phi}}\hat{\boldsymbol{\Lambda}} & \hat{\boldsymbol{\Phi}}^*\hat{\boldsymbol{\Lambda}}^* \end{bmatrix} \in \mathbb{C}^{2n \times 2r}. \tag{19}$$

In addition to the conditions (16)–(18), constraints are introduced to keep the structural properties of the updated FE matrices, namely the positive-definiteness, the symmetry and the sparsity. To this end, it is first assumed that the FEM matrices can be rewritten as follows:

$$\mathbf{M}_N = \sum_{i=1}^{n_m} \mathbf{M}_i m_i, \quad \mathbf{K}_N = \sum_{i=1}^{n_k} \mathbf{K}_i k_i, \quad \mathbf{C}_N = \sum_{i=1}^{n_c} \mathbf{C}_i c_i. \tag{20}$$

For the considered application, Eqs. (3)–(5) and (6) can readily be rewritten in the form (20) with

$$m_i = m_{1|i}, \quad k_i = k_{1|i}, \quad c_i = c_{1|i} \tag{21}$$

and for $i = 1, 2, \ldots, (n-1)$

$$\mathbf{M}_i = \mathbf{C}_i = \frac{1}{6} \begin{bmatrix} \mathbf{0}_{i-1} & & & \\ & 2 & 1 & \\ & 1 & 2 & \\ & & & \mathbf{0}_{n-i-1} \end{bmatrix}, \quad \mathbf{K}_i = \begin{bmatrix} \mathbf{0}_{i-1} & & & \\ & 1 & -1 & \\ & -1 & 1 & \\ & & & \mathbf{0}_{n-i-1} \end{bmatrix}. \tag{22}$$

Note that the representation in Eq. (20) is rather general and can be applied to a wide variety of practical problems. In this way those quantities in the FEM matrices that can undergo changes and need to be monitored are "pulled out", i.e. the m_i's, k_i's and c_i's, so that the matrices $\{\mathbf{M}_i, \mathbf{C}_i, \mathbf{K}_i\}$ are constant and known. In fact, in many practical situations, these matrices will be symmetric and positive definite, so that

$$\begin{aligned} m_i \geqslant 0,\ \forall i, \quad &\Longrightarrow \mathbf{M} \geqslant 0, \\ k_i \geqslant 0,\ \forall i, \quad &\Longrightarrow \mathbf{K} \geqslant 0, \\ c_i \geqslant 0,\ \forall i, \quad &\Longrightarrow \mathbf{C} \geqslant 0. \end{aligned} \tag{23}$$

Hence, the considered structural constraints on the FEM matrices are represented by Eqs. (20)–(23). Substitution of these into our original conditions (16)–(18) leads to

$$\sum_{i=1}^{n_m} \mathbf{M}_i \hat{\boldsymbol{\Phi}} \hat{\boldsymbol{\Lambda}}^2 m_i + \sum_{i=1}^{n_c} \mathbf{C}_i \hat{\boldsymbol{\Phi}} \hat{\boldsymbol{\Lambda}} c_i + \sum_{i=1}^{n_k} \mathbf{K}_i \hat{\boldsymbol{\Phi}} k_i \approx 0, \tag{24}$$

$$\hat{\boldsymbol{\psi}}_q^{\mathrm{T}} \begin{bmatrix} \sum_{i=1}^{n_c} \mathbf{C}_i c_i & \sum_{i=1}^{n_m} \mathbf{M}_i m_i \\ \sum_{i=1}^{n_m} \mathbf{M}_i m_i & 0 \end{bmatrix} \hat{\boldsymbol{\psi}}_j \approx 0, \quad \forall j \neq q. \tag{25}$$

$$\hat{\boldsymbol{\psi}}_q^{\mathrm{T}} \begin{bmatrix} \sum_{i=1}^{n_k} \mathbf{K}_i k_i & 0 \\ 0 & -\sum_{i=1}^{n_m} \mathbf{M}_i m_i \end{bmatrix} \hat{\boldsymbol{\psi}}_j \approx 0, \quad \forall j \neq q, \tag{26}$$

$$m_i \geqslant 0, \quad k_i \geqslant 0, \quad c_i \geqslant 0, \quad \forall i. \tag{27}$$

Generally speaking, the idea pursued in this paper is to update the FE matrices in such a way that a weighted combination of the Frobenius norms of (24)–(26) is minimized while at the same time the positivity constraints (27) are satisfied. Since the conditions (24)–(26) are complex due to the complex modal parameters, we will

proceed by transforming them into an equivalent set of real conditions. For that purpose, denote

$$\hat{\mathbf{\Phi}}_M = [\mathrm{Re}(\hat{\mathbf{\Phi}}\hat{\mathbf{\Lambda}}^2), \mathrm{Im}(\hat{\mathbf{\Phi}}\hat{\mathbf{\Lambda}}^2)] = [\hat{\boldsymbol{\phi}}_{M,1}, \ldots, \hat{\boldsymbol{\phi}}_{M,2r}],$$

$$\hat{\mathbf{\Phi}}_C = [\mathrm{Re}(\hat{\mathbf{\Phi}}\hat{\mathbf{\Lambda}}), \mathrm{Im}(\hat{\mathbf{\Phi}}\hat{\mathbf{\Lambda}})] = [\hat{\boldsymbol{\phi}}_{C,1}, \ldots, \hat{\boldsymbol{\phi}}_{C,2r}],$$

$$\hat{\mathbf{\Phi}}_K = [\mathrm{Re}(\hat{\mathbf{\Phi}}), \mathrm{Im}(\hat{\mathbf{\Phi}})] = [\hat{\boldsymbol{\phi}}_{K,1}, \ldots, \hat{\boldsymbol{\phi}}_{K,2r}]. \tag{28}$$

With this notation at hand, it is not difficult to see that conditions (24)–(26) can be rewritten as

$$\mathbf{J}^{(1)} = \sum_{i=1}^{n_m} (\mathbf{M}_i \hat{\mathbf{\Phi}}_M) m_i + \sum_{i=1}^{n_c} (\mathbf{C}_i \hat{\mathbf{\Phi}}_C) c_i + \sum_{i=1}^{n_k} (\mathbf{K}_i \hat{\mathbf{\Phi}}_K) k_i \approx 0, \tag{29}$$

$$J_{jq}^{(2)} = \sum_{i=1}^{n_c} (\hat{\boldsymbol{\phi}}_{K,j}^{\mathrm{T}} \mathbf{C}_i \hat{\boldsymbol{\phi}}_{K,q}) c_i + \sum_{i=1}^{n_m} (\hat{\boldsymbol{\phi}}_{C,j}^{\mathrm{T}} \mathbf{M}_i \hat{\boldsymbol{\phi}}_{K,q} + \hat{\boldsymbol{\phi}}_{K,j}^{\mathrm{T}} \mathbf{M}_i \hat{\boldsymbol{\phi}}_{C,q}) m_i \approx 0, \tag{30}$$

$$J_{jq}^{(3)} = \sum_{i=1}^{n_k} (\hat{\boldsymbol{\phi}}_{K,j}^{\mathrm{T}} \mathbf{K}_i \hat{\boldsymbol{\phi}}_{K,q}) k_i - \sum_{i=1}^{n_m} (\hat{\boldsymbol{\phi}}_{C,j}^{\mathrm{T}} \mathbf{M}_i \hat{\boldsymbol{\phi}}_{C,q}) m_i \approx 0. \tag{31}$$

Then the optimization problem is defined as follows:

$$\underset{\mathbf{m}\geqslant 0, \mathbf{c}\geqslant 0, \mathbf{k}\geqslant 0}{\text{minimize}} \ \|\mathbf{J}^{(1)}\|_F^2 + \sum_{j\neq q} (\alpha |J_{jq}^{(2)}|^2 + \beta |J_{jq}^{(3)}|^2), \tag{32}$$

where α and β are two non-negative weighting scalars that can be used to achieve some desired trade-off between the three different objectives, and where it is denoted

$$\mathbf{m} = [m_1, \ldots, m_{n_m}]^{\mathrm{T}}, \quad \mathbf{c} = [c_1, \ldots, c_{n_c}]^{\mathrm{T}}, \quad \mathbf{k} = [k_1, \ldots, k_{n_k}]^{\mathrm{T}}. \tag{33}$$

This optimization problem is easily transformed into a standard least-squares optimization problem of the form (see Appendix A for details)

$$\underset{\mathbf{m}\geqslant 0, \mathbf{c}\geqslant 0, \mathbf{k}\geqslant 0}{\text{minimize}} \ \|\mathbf{U}_M \mathbf{m} + \mathbf{U}_c \mathbf{c} + \mathbf{U}_K \mathbf{k}\|_2^2, \tag{34}$$

where $\mathbf{U}_M$, $\mathbf{U}_C$ and $\mathbf{U}_K$ are known matrices.

Remark 1. Clearly, the optimization problem (34) allows an analytic solution in the case there are no positivity constraints. In fact, since the true FEM parameters are positive and achieve a value of zero for the cost function when the true modal parameters are used in the optimization, one can actually expect that, if the estimates of the modal parameters are accurate enough, the unconstrained solution of Eq. (34) will be non-negative. The difficulty here is that the estimated modal parameters are never that accurate, so that the unconstrained solution cannot be guaranteed to be positive. If it is not positive, one can use it to initialize an active set algorithm, see for instance Ref. [21]. We point out that the active set algorithm computes the *exact* constrained solution in a finite number of iterations. The MatLab function lsqlin from the Optimization toolbox also efficiently implements such an algorithm.

Note that multiplication of Eq. (7) with a positive scalar results in different FEM matrices that have the same structure and produce the same output $\mathbf{y}(t)$. Therefore, given only output measurements, no method will be able to uniquely estimate all entries in the FEM, not even by exploiting the structural properties of the FEM model (i.e. symmetry, positive-definiteness, connectivity). To circumvent this problem, the so-called reference basis methods [4,7,13] usually assume that either one of the three matrices is known (or remains unchanged), or that the mode shapes $\mathbf{\Phi}$ are exact and are mass-normalized, i.e. $\mathbf{\Phi}^{\mathrm{T}}\mathbf{M}\mathbf{\Phi} = \mathbf{I}$. The later assumption is obviously not practical when the mass matrix can also undergo changes as a result of damage. In this paper we circumvent this non-uniqueness problem by assuming that only one (or at most a few) matrix entry, say $m_{1|1}$, remains unchanged. With a few fixed entries of $\mathbf{m}$, $\mathbf{c}$ and/or $\mathbf{k}$, the optimization problem (34) takes the form $\min \|\mathbf{A}\mathbf{x} + \mathbf{b}\|_2^2$, where the new variable $\mathbf{x}$ contains the unknown (free) entries of the vectors $\mathbf{m}$, $\mathbf{c}$

and **k**. In most practical problems the matrix **A** will be left-invertible, so that the optimal solution is indeed unique. If **A** turns out not to be full column rank for some specific problem, one can either consider using some more modal estimates or fixing some other entries of **m**, **c** and/or **k**.

Another way to circumvent the problem of non-uniqueness is to add up another term to the cost function (32) that penalizesany change of the vectors **m**, **c** and **k** from their nominal values, i.e.

$$\underset{\mathbf{m}\geqslant 0,\mathbf{c}\geqslant 0,\mathbf{k}\geqslant 0}{\text{minimize}} \|\mathbf{U}_M\mathbf{m}+\mathbf{U}_c\mathbf{c}+\mathbf{U}_K\mathbf{k}\|_2^2+\delta\left\|\begin{bmatrix}\mathbf{m}-m_{\text{nom}}\\ \mathbf{k}-k_{\text{nom}}\\ \mathbf{c}-c_{\text{nom}}\end{bmatrix}\right\|_2^2. \tag{35}$$

The weight δ is usually a small positive number, as otherwise the second term would become significant and will push the optimal solution towards the nominal values of the parameters.

4. Experimental results

In this section, both experimental and simulation results are presented and the FEMU algorithm is compared to some other existing methods based on FEM updating. The test scenarios are explained in Section 2.2.

The starting point is the measured vibration data. In order to estimate the modal parameters, a state–space model is first identified using a Subspace Model Identification method [22]. When the input signal is not measured the stochastic subspace identification methods [23,24] can be used instead to identify a state–space model. Subsequently, the modal parameters for the first five modes are computed from the state–space model at the dof where the sensors are located. These are next expanded using B-spline approximation method. Once the modal parameters are estimated at all dof, the method discussed in Section 3.2 is applied to identify the size and the location of the changed structural parameter(s). The results obtained are compared to a number of other algorithms in order to highlight the superiority of the new method presented. In the following subsections, these steps are described in more detail.

4.1. Step 1: subspace model identification

The first step is to identify a state–space model of the structure. For each test scenario performed, input-output measurement data is collected for 300 s at a sampling frequency of 2048 Hz, coming up to a total of 614 400 data points per sensor per test scenario. In order to process this huge amount of data, it was first split into 20 data batches. Since the input signal is a frequency sweep, one cannot just use one such data batch to identify the model, because in such a case the data will represent only a narrow frequency range. For that reason, the whole data has been used for model identification. The problem with the data dimension was been circumvented by making use of the subspace model identification (SMI) toolbox [25], that has the ability to process all the data by iteratively processing the different data batches.

The Bode magnitude plots of the identified state–space models for the four test scenarios considered, explained in Section 2.2, are plotted in Fig. 5 (the dashed lines). Also plotted, for comparison, is the Bode magnitude plots obtained from the analytical model of the cable. On the vertical axis the magnitude is given in dB (i.e. $20\log_{10}$(magnitude)).

4.2. Step 2: Modal parameters computation

A state–space model corresponding to the FEM (1) is

$$\begin{bmatrix}\dot{\mathbf{x}}(t)\\ \ddot{\mathbf{x}}(t)\end{bmatrix}=\begin{bmatrix}\mathbf{0} & \mathbf{I}\\ -\mathbf{M}^{-1}\mathbf{K} & -\mathbf{M}^{-1}\mathbf{C}\end{bmatrix}\begin{bmatrix}\mathbf{x}(t)\\ \dot{\mathbf{x}}(t)\end{bmatrix}+\begin{bmatrix}\mathbf{0}\\ \mathbf{M}^{-1}\mathbf{B}\end{bmatrix}\mathbf{F}_m(t),$$

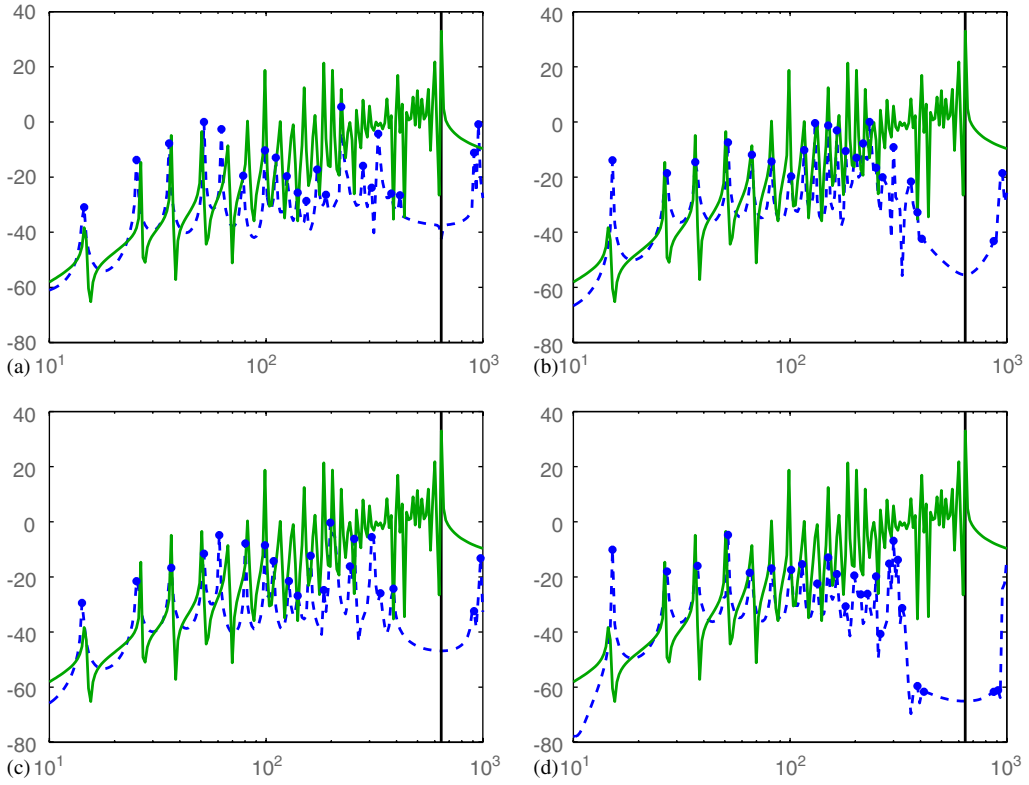

Fig. 5. Bode magnitude plots (magnitude [dB] vs. frequency [Hz]) of the analytical model (solid line) and the identified model (dashed line) for the four considered test scenarios: (a) Case 1, (b) Case 2, (c) Case 3 and (d) Case 4.

$$\mathbf{y}(t) = [-\mathbf{C}_a\mathbf{M}^{-1}\mathbf{K} \quad -\mathbf{C}_a\mathbf{M}^{-1}\mathbf{C}]\begin{bmatrix}\mathbf{x}(t)\\ \dot{\mathbf{x}}(t)\end{bmatrix}. \tag{36}$$

From the state–space model one can compute the modal parameters from the eigenvalue decomposition, since the following holds:

$$\begin{bmatrix}\mathbf{0} & \mathbf{I}\\ -\mathbf{M}^{-1}\mathbf{K} & -\mathbf{M}^{-1}\mathbf{C}\end{bmatrix}\begin{bmatrix}\boldsymbol{\Phi}\\ \boldsymbol{\Phi}\boldsymbol{\Lambda}\end{bmatrix} = \begin{bmatrix}\boldsymbol{\Phi}\\ \boldsymbol{\Phi}\boldsymbol{\Lambda}\end{bmatrix}\boldsymbol{\Lambda}. \tag{37}$$

In this way, one could estimate the modal parameters at all dof. The problem is, however, that the identified state–space model is not necessarily in the same state basis, so that also the mode shapes are in a different basis (the eigenvalues are invariant to the state basis). Indeed, with any nonsingular transformation matrix $\mathbf{T}$, one rewrites Eq. (37) as

$$\underbrace{\left(\mathbf{T}\begin{bmatrix}\mathbf{0} & \mathbf{I}\\ -\mathbf{M}^{-1}\mathbf{K} & -\mathbf{M}^{-1}\mathbf{C}\end{bmatrix}\mathbf{T}^{-1}\right)}_{\text{estimated } \mathbf{A} \text{ matrix}}\underbrace{\left(\mathbf{T}\begin{bmatrix}\boldsymbol{\Phi}\\ \boldsymbol{\Phi}\boldsymbol{\Lambda}\end{bmatrix}\right)}_{\text{eigenvectors}} = \left(\mathbf{T}\begin{bmatrix}\boldsymbol{\Phi}\\ \boldsymbol{\Phi}\boldsymbol{\Lambda}\end{bmatrix}\right)\boldsymbol{\Lambda}. \tag{38}$$

From the estimated $\mathbf{A}$ matrix it is difficult to compute the state transformation matrix $\mathbf{T}$ which is needed to transform the mode shapes into the original basis. However, at the dof where the sensors are located the mode

shapes can be correctly estimated without knowing $\mathbf{T}$ by observing that

$$\overbrace{([-\mathbf{C}_a\mathbf{M}^{-1}\mathbf{K} \quad -\mathbf{C}_a\mathbf{M}^{-1}\mathbf{C}]\mathbf{T}^{-1})}^{\text{estimated c matrix}}\left(\mathbf{T}\begin{bmatrix}\boldsymbol{\Phi}\\ \boldsymbol{\Phi}\boldsymbol{\Lambda}\end{bmatrix}\right)$$
$$=\underbrace{[-\mathbf{C}_a\mathbf{M}^{-1}\mathbf{K} \quad -\mathbf{C}_a\mathbf{M}^{-1}\mathbf{C}]}_{\text{original c matrix}}\begin{bmatrix}\boldsymbol{\Phi}\\ \boldsymbol{\Phi}\boldsymbol{\Lambda}\end{bmatrix}=\hat{\boldsymbol{\Phi}}_{\text{sen}}, \tag{39}$$

where $\hat{\boldsymbol{\Phi}}_{\text{sen}}$ is defined as follows:

$$\hat{\boldsymbol{\Phi}}_{\text{sen}}=\begin{bmatrix}\hat{\phi}_{j_1,1} & \hat{\phi}_{j_1,2} & \cdots & \hat{\phi}_{j_1,r}\\ \hat{\phi}_{j_2,1} & \hat{\phi}_{j_2,2} & \cdots & \hat{\phi}_{j_2,r}\\ \vdots & \vdots & \ddots & \vdots\\ \hat{\phi}_{j_l,1} & \hat{\phi}_{j_l,2} & \cdots & \hat{\phi}_{j_l,r}\end{bmatrix} \tag{40}$$

with $\{j_1,j_2,\ldots,j_l\}$ representing the dof where the sensors are located.

To summarize, the subspace identification method estimates a linear discrete-time model of the form

$$\mathbf{x}_{d,k+1}=\mathbf{A}_d\mathbf{x}_{d,k}+\mathbf{B}_d\mathbf{F}_{m,k},$$
$$\mathbf{y}_k=\mathbf{C}_d\mathbf{x}_{d,k} \tag{41}$$

from which the mode shapes and eigenvectors (of the continuous-time system) are computed from the eigenvalue decomposition of $\mathbf{A}_d$

$$\mathbf{A}_d=\mathbf{U}\boldsymbol{\Lambda}_d\mathbf{U}^{-1}. \tag{42}$$

Here, $\mathbf{U}$ represent the mode shapes in some unknown state basis $\mathbf{T}$. To get rid of $\mathbf{T}$, they are related to the sensor locations as follows:

$$\hat{\boldsymbol{\Phi}}_{\text{sen}}=\mathbf{C}_d\mathbf{U}. \tag{43}$$

$\hat{\boldsymbol{\Phi}}_{\text{sen}}$ is subsequently expanded using B-spline approximation method. For that purpose, Matlab's Spline Toolbox [26] has been used.

Note that, unlike the eigenvalues, the mode shapes are the same for the continuous and discrete-time models. The eigenvalues for the continuous-time model are computed from $\boldsymbol{\Lambda}_d$ using the relation

$$\hat{\lambda}_i=\frac{\log\lambda_{d,i}}{T_s}, \tag{44}$$

where $\lambda_{d,i}$ is the ith diagonal element of $\boldsymbol{\Lambda}_d$ and T_s is the sampling time.

Fig. 6 depicts the mode shapes corresponding to the first five modes, computed for the first four test scenarios, see Section 2.2.1. These four test scenarios are represented by the four columns. Both the real part and the imaginary parts are plotted. Each plot depicts the corresponding mode shape as computed from the nominal (damage-free) analytical model of the cable (the dashed lines), the mode shape estimates at the sensor locations $\hat{\boldsymbol{\Phi}}_{\text{sen}}$ (the nine dots), and spline interpolation of the mode shapes $\hat{\boldsymbol{\Phi}}$ which is subsequently used in the FEMU methods (the solid lines). We point out that the spline interpolation is particularly suitable for the considered case study as the mode shapes possess certain smoothness properties. Similar is the case with beams, masts, plates and other less complex structures are considered, where mode shape expansion techniques based on smoothing curves approximations can also be useful. For general structures, however, the application of the spline approximation method should be applied with care, possibly only locally at certain (smooth) parts of the structure and in combination with other existing mode shape expansion methods.

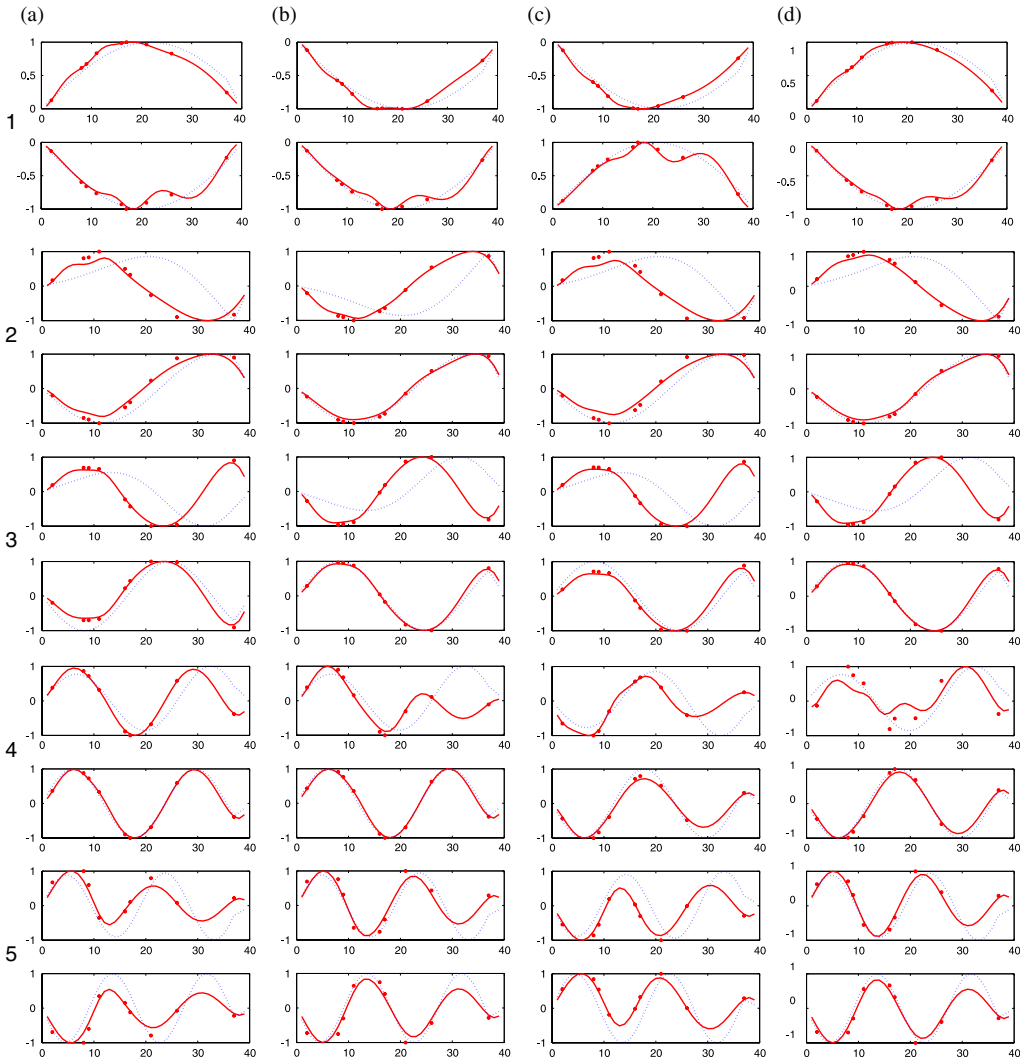

Fig. 6. Real and imaginary parts of the first five mode shapes for the four considered test scenarios: computed using the nominal analytical model (dashed line), the estimates at the sensor locations $\hat{\mathbf{\Phi}}_{\text{sen}}$ (the bigger dots), and the B-spline approximations $\hat{\mathbf{\Phi}}$ (solid line). The ith row depicts the ith mode shape, while the columns represent the four test scenarios: (a) Case 1, (b) Case 2, (c) Case 3 and (d) Case 4. The upper graph of each row–column pair represents the real part of the corresponding mode shape, while the lower graph—the imaginary part.

4.3. Step 3: Finite-element model updating

The FEMU algorithm, proposed in this paper, is applied to the estimated modal parameters. The results are presented in this subsection. It is assumed that only m_1 is fixed and the remaining entries of $\mathbf{m}$, as well as the whole vectors $\mathbf{k}$ and $\mathbf{c}$, have to be estimated. Besides the new method, which is used to optimize the cost function (32) with $\alpha = \beta = 1$, thirteen different other methods have been implemented and run on the data so that a comparison could be made. These algorithms are summarized in Table 5, where their abbreviations, names, main assumptions, and references, where the methods are described, are reported. Interestingly, none of these methods is suited for any of the damage cases considered in this paper where the M matrix changes, the damping matrix is present in the FEM, and the identified mode shapes are not mass-normalized.

Table 5
Compared FEMU-based algorithms

Abbr.	Name	Ass.	Refs.
AP	Alternative Projection Method	$\mathbf{M} = \text{const.}, \mathbf{C} = 0$	[10]
Baruch	Baruch Algorithm	$\mathbf{M} = \text{const.}, \mathbf{C} = 0$	[14,3]
BBI	Baruch & Bar Itzhack Algorithm	$\mathbf{M} = \text{const.}, \mathbf{C} = 0$	[10]
BN	Algorithm of Berman & Nagy	$\hat{\mathbf{\Phi}}^{\mathrm{T}}\mathbf{M}\hat{\mathbf{\Phi}} = I, \mathbf{C} = 0$	[6,3]
Caesar	Algorithm of Caesar	$\hat{\mathbf{\Phi}}^{\mathrm{T}}\mathbf{M}\hat{\mathbf{\Phi}} = I, \mathbf{C} = 0$	[3]
Chen	Algorithm of Chen	$\mathbf{C} = 0$	[6]
Friswell	Algorithm of Friswell	$\mathbf{M} = \text{const.}$	[7]
Gysin	Algorithm of Gysin	$\hat{\mathbf{\Phi}}^{\mathrm{T}}\mathbf{M}\hat{\mathbf{\Phi}} = I, \mathbf{C} = 0$	[3]
HB	Halevi & Bucher Algorithm	$\mathbf{M} = \text{const.}, \mathbf{C} = 0$	[13]
KH	Kenigsbuch and Halevi Algorithm	$\hat{\mathbf{\Phi}}^{\mathrm{T}}\mathbf{M}\hat{\mathbf{\Phi}} = I, \mathbf{C} = 0$	[4]
OFEA	Output Feedback Eigenstr. Ass.	$\mathbf{M} = \text{const.}$	[3]
SFEA	State Feedback Eigenstr. Ass.	$\mathbf{M} = \text{const.}$	[17]
Wei	Algorithm of Wei	$\hat{\mathbf{\Phi}}^{\mathrm{T}}\mathbf{M}\hat{\mathbf{\Phi}} = I, \mathbf{C} = 0$	[3]

4.3.1. Local mass changes

To begin with, test scenarios 1–4 are considered (see Section 2.2.1 and Table 2), where only local changes in some mass element are introduced. The damping and stiffness remain unchanged. Note that algorithms AP, Baruch, BBI, Friswell, HB, OFEA, SFEA assume that the mass matrix remains unchanged, and therefore these cannot detect the changes in the mass matrix, introduced in the four test scenarios. The results from these methods are therefore not plotted in order not to increase the number of lines unnecessarily, which would only reduce the readability. Hence, in Figs. 7 and 8, only the results obtained with the new method and with methods BN, Chen, KH, Caesar, and Gysin are reported. Fig. 7 depicts the 39 elements on the first main diagonal (see first column) and the 38 elements of the second main diagonal (see second column) of the mass matrix, as estimated by these methods. Additionally, the analytical elements have also been plotted (the dashed curve) and are considered as the "true" values. We remark that the high peaks after node 35 are due to the shaker, located at 37, which introduces a large fictitious mass at that point. This mass is unknown and much larger than the masses of the finite elements. The plots are suitably zoomed so that the region of interest is best visualized, namely the region up to node 35.

Close inspection of Fig. 7 reveals the following:

- For all four test scenarios the proposed approach (solid line) gives the best estimates of the "true" parameters (dashed line). The methods Chen and Gysin are rather insensitive to the increased mass and provide no means of even detecting the damage. The methods BN, KH and Caesar are clearly able to detect damage in the cable. However, these methods seem to be unable to accurately enough identify the mass matrix elements—they result in overly conservative estimates that are way larger than the true values. The new method clearly outperformed the other methods providing the best estimates throughout all nodes.
- The proposed method detects the changes in the mass for all four test scenarios. At first sight, there are also certain points where false alarms could be triggered, e.g. around nodes 2, 10 and 25. Hence, it is clear that the small masses are much more difficult to identify.

The estimates of the diagonal elements of the stiffness matrix $\mathbf{K}$ are also reported, see Fig. 8. All methods perform equally well and detect no change there, the deviations from the nominal values being smaller within 10% (only the method Caesar, and may be KH, detect incorrectly a decrease in the stiffness around node 37).

To even more closely compare the methods, Table 6 is provided. The first three columns of the table report whether or not the algorithms preserve the structural properties of the FEM, namely the symmetry of the updated matrices, their original sparsity/connectivity, and their positive-definiteness. Besides the new method, only two of the other compared algorithms preserve all the three of these properties, namely AP and HB.

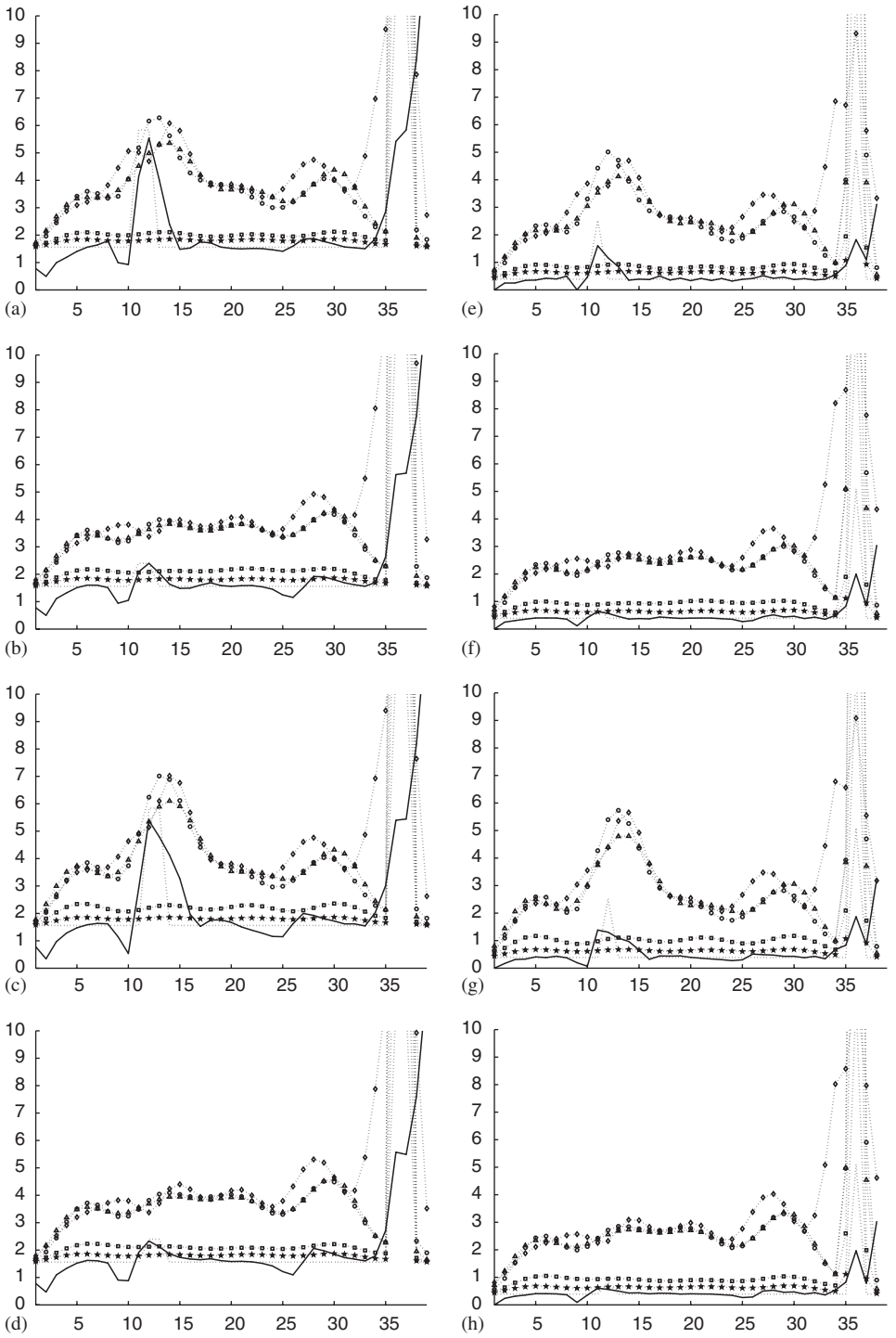

Fig. 7. Plots of the elements on the main diagonal (a–d) and the second main diagonal (e–h) of the FEM matrix M (kg). The four rows represent the four test scenarios: (a),(e) Case 1; (b),(f) Case 2; (c),(g) Case 3 and (d),(h) Case 4. The lines on the plots represent the following methods: true mass (dashed lines), new method (solid lines), BN (○-marked lines), Chen (□-marked lines), KH (⋆-marked lines), Caesar (△-marked lines), and Gysin (◇-marked lines).

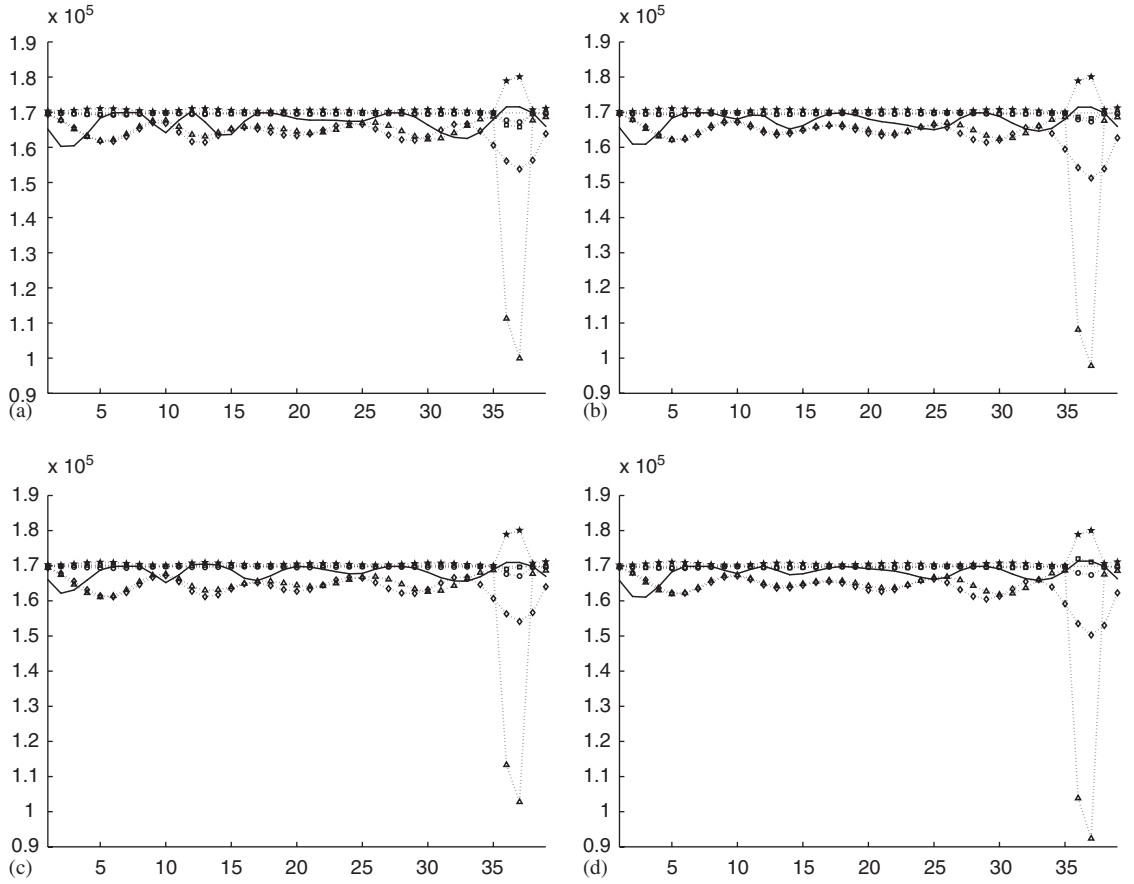

Fig. 8. Plots of the elements on the main diagonal of the FEM matrix **K** (N/m) for the four considered test scenarios: (a) Case 1, (b) Case 2, (c) Case 3 and (d) Case 4. The lines on the plots represent the following methods: true mass (dashed lines), new method (solid lines), BN (○-marked lines), Chen (□-marked lines), KH (⋆-marked lines), Caesar (△-marked lines), and Gysin (◇-marked lines).

Table 6
Comparison of the methods for the four different test scenarios using the cost function (45)

Alg	Sym	Sprs	>0	Case 1	Case 2	Case 3	Case 4
NEW	Yes	Yes	Yes	5.94×10^5	7.09×10^5	7.15×10^5	6.4×10^5
AP	Yes	Yes	Yes	1.93×10^{19}	1.99×10^{19}	1.48×10^{19}	1.48×10^{19}
Baruch	No	No	Yes	7.74×10^6	7.96×10^6	7.58×10^6	7.17×10^6
BBI	No	No	No	4.43×10^7	4.31×10^7	5.31×10^7	5.07×10^7
BN	Yes	No	Yes	5.5×10^8	5.52×10^8	5.86×10^8	6.25×10^8
Caesar	Yes	No	No	2.79×10^9	2.77×10^9	2.83×10^9	$3. \times 10^9$
Chen	Yes	No	Yes	5.59×10^7	6.11×10^7	6.76×10^7	6.36×10^7
Friswell	No	No	No	7.79×10^{11}	9.46×10^{11}	1.46×10^{14}	1.38×10^{13}
Gysin	No	No	Yes	1.18×10^7	1.19×10^7	8.41×10^6	8.05×10^6
HB	Yes	Yes	Yes	5.99×10^6	5.96×10^6	4.84×10^6	4.63×10^6
KH	No	No	No	2.13×10^9	2.14×10^9	2.27×10^9	2.38×10^9
OFEA	No	No	Yes	6.57×10^6	6.56×10^6	5.61×10^6	5.3×10^6
SFEA	No	No	No	1.78×10^{10}	5.04×10^{10}	1.92×10^{10}	7.52×10^9
Wei	No	No	No	2.92×10^{32}	1.94×10^{32}	7.03×10^{32}	7.07×10^{32}

Furthermore, the algorithms are compared with respect to whether or not they preserve the structural properties of the FEM: symmetry (sym), sparsity (sprs) and positivity (>0).

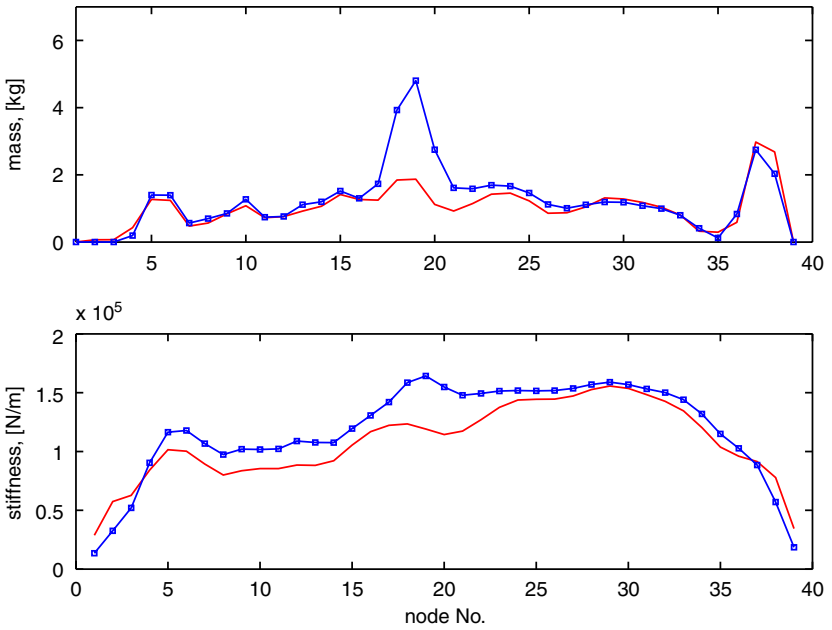

Fig. 9. Results with experimental test scenarios 5 (nominal, solid line) and 6 (local mass and global stiffness increase, □-marked line).

Furthermore, the table reports the values of the cost function

$$J = \|\mathbf{M}\hat{\mathbf{\Phi}}\hat{\mathbf{\Lambda}}^2 + \mathbf{C}\hat{\mathbf{\Phi}}\hat{\mathbf{\Lambda}} + \mathbf{K}\hat{\mathbf{\Phi}}\|_F^2 \tag{45}$$

computed with the estimated FEM by the different methods for the four considered test scenarios. Clearly, the new method outperforms the other methods by achieving the smallest values for this cost function for all test scenarios. Although not reported in this paper for the sake of brevity, a comparison with respect to the cost function (32) led to a similar conclusion.

4.3.2. *Local mass and global cable tension change*

Next, test scenarios 5 and 6 are considered, where test scenario 5 will represent nominal case, and 6 represents damage resulting in a local mass increase at node 19 and a (global) cable tension increase, see Table 3. Note that the cable tension T directly affects the stiffness matrix as can be seen from Eq. (6). Therefore, besides an increase in m_{19}, we should also be able to observe an increase in the entries estimated vector $\mathbf{k}$ or, equivalently, in the diagonal elements of the matrix $\mathbf{K}$. Indeed, this is what is observed in Fig. 9. Observe that the mass change at node 19 is again very clearly identifiable. The change in the stiffness can also be easily detected by noting the increase diagonal elements of the matrix $\mathbf{K}$.

For these test scenarios 5 and 6 no comparison study with the other methods is reported in the paper as the results are similar to those reported already in the previous subsection.

4.3.3. *Simulation of local changes in* $\boldsymbol{m}$, $\boldsymbol{k}$ *and* $\boldsymbol{c}$

Finally, we consider a simulation that allows us to validate the performance of the novel method on idealistic data (the modal parameters are exactly known at all dof), but in the presence of local changes in both mass, stiffness and damping. The experimental setup does not make it possible to implement such changes. However, even though this simulation might be of less interest than the experimental results reported above, it serves as a good basis for another comparison study between the discussed methods in the case when the modal parameters are given.

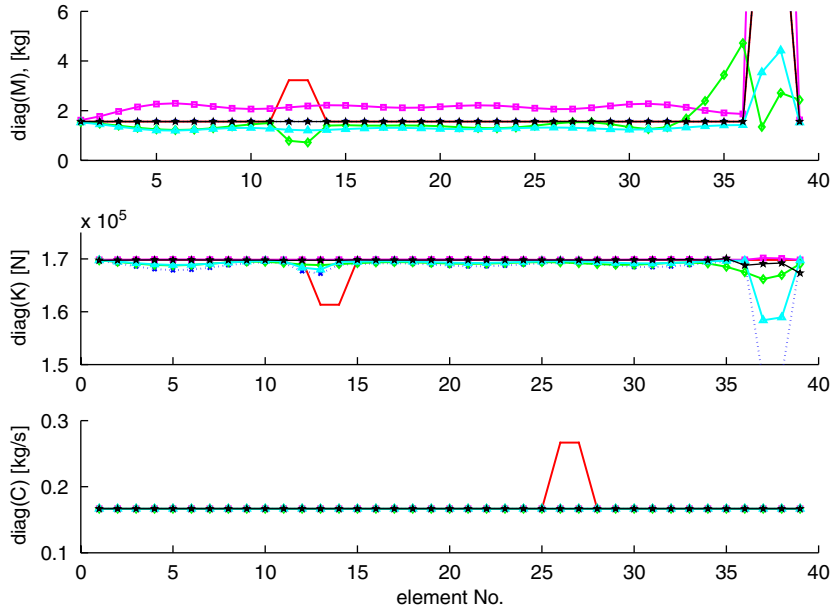

Fig. 10. Results with simulation test scenario 7 (local changes in m_{12}, k_{13} and c_{26}). The lines on the plots represent the following methods: new method (solid lines), BBI (dotted lines), Chen (□-marked lines), KH (◇-marked lines), Caesar (▲-marked lines), and HB (⋆-marked lines).

The damage FEM model in this case was formed from Eqs. (3)–(6), with the nominal parameters given in Table 1, and with additional local changes of $m_{:|12}$, $k_{:|13}$ and $c_{:|26}$, summarized in Table 4.

Fig. 10 depicts the elements on the main diagonals of the matrices **M**, **K** and **C**, respectively, estimated by the compared methods. Note that besides the new method, only the results with the methods BBI, Chen, KH, Caesar and HB are presented; the remaining discussed methods have also been tested but resulted very poor estimates.

The method that best performs on this simulation data is again the novel method considered (solid line), which was capable to exactly detect the changes in the structural parameters. The true values of the entries on the main diagonals of the three FEM matrices coincide with the three solid lines on Fig. 10. Note that no other method was capable to even closely approximate the simulated changes. Clearly, for the damage cases considered, those methods are much less reliable than the new method. This is due to the fact that the assumptions that the other methods make (see Table 5) are too restrictive and do not apply to the test scenarios considered here.

5. Conclusion

This paper summarizes a new approach to damage identification and experimentally validates it on a problem of damage localization. The starting point of the method is the availability of modal parameters of the first several modes, which are then used in a novel finite element model updating (FEMU) method that computes the structural parameters of the system. In this method the finite element model (FEM) matrices are updated to match best the modal data in terms of the quadratic eigenvalue problem and a pair of generalized orthogonality conditions. The advantage of this new approach is its ability to simultaneously update all three FEM matrices and that it explicitly takes into account the structural constraints, namely the sparsity (connectivity) of the matrices, their symmetry and positive-definiteness. A comparison with a number of other existing FEMU methods is made to confirm the superiority of the newly proposed method.

Acknowledgments

This work is partially sponsored by the integrated European Union project "Intelligent Materials for Active Noise Reduction" (InMAR).

The authors also gratefully acknowledge the technical support of the staff of the Structural Engineering Research Laboratory, and the financial support of the Swiss Federal Laboratories for Materials Testing and Research (EMPA), Switzerland.

Appendix A. Least-squares formulation

The optimization problem (32) is easily transformed into a standard least-squares problem with positivity constraints by observing that

$$\|\mathbf{J}^{(1)}\|_F^2 = \|\mathbf{vec}(\mathbf{J}^{(1)})\|_2^2 = \|\mathbf{U}_M^{(1)}\mathbf{m} + \mathbf{U}_C^{(1)}\mathbf{c} + \mathbf{U}_K^{(1)}\mathbf{k}\|_2^2 \tag{A.1}$$

with

$$\begin{aligned}
\mathbf{U}_M^{(1)} &= [\mathbf{vec}(\mathbf{M}_1\hat{\mathbf{\Phi}}_M), \ldots, \mathbf{vec}(\mathbf{M}_{n_m}\hat{\mathbf{\Phi}}_M)],\\
\mathbf{U}_C^{(1)} &= [\mathbf{vec}(\mathbf{C}_1\hat{\mathbf{\Phi}}_C), \ldots, \mathbf{vec}(\mathbf{C}_{n_c}\hat{\mathbf{\Phi}}_C)],\\
\mathbf{U}_K^{(1)} &= [\mathbf{vec}(\mathbf{K}_1\hat{\mathbf{\Phi}}_K), \ldots, \mathbf{vec}(\mathbf{K}_{n_k}\hat{\mathbf{\Phi}}_K)].
\end{aligned} \tag{A.2}$$

Furthermore,

$$\begin{aligned}
\sum\nolimits_{j\neq q} |J_{jq}^{(2)}|^2 &= \|\mathbf{U}_M^{(2)}\mathbf{m} + \mathbf{U}_C^{(2)}\mathbf{c}\|_2^2,\\
\sum_{j\neq q} |J_{jq}^{(3)}|^2 &= \|\mathbf{U}_M^{(3)}\mathbf{m} + \mathbf{U}_K^{(3)}\mathbf{k}\|_2^2,
\end{aligned} \tag{A.3}$$

where

$$\mathbf{U}_M^{(2)} = \begin{bmatrix} \mathbf{U}_{M,12}^{(2)} \\ \mathbf{U}_{M,13}^{(2)} \\ \vdots \\ \mathbf{U}_{M,1r}^{(2)} \\ \mathbf{U}_{M,23}^{(2)} \\ \vdots \\ \mathbf{U}_{M,2r}^{(2)} \\ \vdots \\ \mathbf{U}_{M,(r-1)r}^{(2)} \end{bmatrix}, \quad \mathbf{U}_C^{(2)} = \begin{bmatrix} \mathbf{U}_{C,12}^{(2)} \\ \mathbf{U}_{C,13}^{(2)} \\ \vdots \\ \mathbf{U}_{C,1r}^{(2)} \\ \mathbf{U}_{C,23}^{(2)} \\ \vdots \\ \mathbf{U}_{C,2r}^{(2)} \\ \vdots \\ \mathbf{U}_{C,(r-1)r}^{(2)} \end{bmatrix}, \quad \mathbf{U}_M^{(3)} = \begin{bmatrix} \mathbf{U}_{M,12}^{(3)} \\ \mathbf{U}_{M,13}^{(3)} \\ \vdots \\ \mathbf{U}_{M,1r}^{(3)} \\ \mathbf{U}_{M,23}^{(3)} \\ \vdots \\ \mathbf{U}_{M,2r}^{(3)} \\ \vdots \\ \mathbf{U}_{M,(r-1)r}^{(3)} \end{bmatrix}, \quad \mathbf{U}_C^{(3)} = \begin{bmatrix} \mathbf{U}_{C,12}^{(3)} \\ \mathbf{U}_{C,13}^{(3)} \\ \vdots \\ \mathbf{U}_{C,1r}^{(3)} \\ \mathbf{U}_{C,23}^{(3)} \\ \vdots \\ \mathbf{U}_{C,2r}^{(3)} \\ \vdots \\ \mathbf{U}_{C,(r-1)r}^{(3)} \end{bmatrix},$$

$$\begin{aligned}
\mathbf{U}_{M,jq}^{(2)} &= [\hat{\boldsymbol{\phi}}_{C,j}^{\mathrm{T}}\mathscr{M}_1\hat{\boldsymbol{\phi}}_{K,q}^{\mathrm{T}} + \hat{\boldsymbol{\phi}}_{K,j}^{\mathrm{T}}\mathbf{M}_1\hat{\boldsymbol{\phi}}_{C,q}^{\mathrm{T}}, \ldots, \hat{\boldsymbol{\phi}}_{C,j}^{\mathrm{T}}\mathbf{M}_{n_m}\hat{\boldsymbol{\phi}}_{K,q}^{\mathrm{T}} + \hat{\boldsymbol{\phi}}_{K,j}^{\mathrm{T}}\mathbf{M}_{n_m}\hat{\boldsymbol{\phi}}_{C,q}^{\mathrm{T}}],\\
\mathbf{U}_{C,jq}^{(2)} &= [\hat{\boldsymbol{\phi}}_{K,j}^{\mathrm{T}}\mathbf{C}_1\hat{\boldsymbol{\phi}}_{K,q}, \ldots, \hat{\boldsymbol{\phi}}_{K,j}^{\mathrm{T}}\mathbf{C}_{n_c}\hat{\boldsymbol{\phi}}_{K,q}],\\
\mathbf{U}_{M,jq}^{(3)} &= [\hat{\boldsymbol{\phi}}_{C,j}^{\mathrm{T}}\mathbf{M}_1\hat{\boldsymbol{\phi}}_{C,q}, \ldots, \hat{\boldsymbol{\phi}}_{C,j}^{\mathrm{T}}\mathbf{M}_{n_m}\hat{\boldsymbol{\phi}}_{C,q}], \quad \mathbf{U}_{K,jq}^{(3)} = [\hat{\boldsymbol{\phi}}_{K,j}^{\mathrm{T}}\mathbf{K}_1\hat{\boldsymbol{\phi}}_{K,q}, \ldots, \hat{\boldsymbol{\phi}}_{K,j}^{\mathrm{T}}\mathbf{K}_{n_k}\hat{\boldsymbol{\phi}}_{K,q}].
\end{aligned} \tag{A.4}$$

Therefore, the original cost function (32) takes the form

$$\underset{\mathbf{m}\geqslant 0,\mathbf{c}\geqslant 0,\mathbf{k}\geqslant 0}{\text{minimize}} \left\| \begin{bmatrix} \mathbf{U}_M^{(1)} & \mathbf{U}_C^{(1)} & \mathbf{U}_K^{(1)} \\ \mathbf{U}_M^{(2)} & \mathbf{U}_C^{(2)} & 0 \\ \mathbf{U}_M^{(3)} & 0 & \mathbf{U}_K^{(3)} \end{bmatrix} \begin{bmatrix} \mathbf{m} \\ \mathbf{c} \\ \mathbf{k} \end{bmatrix} \right\|_2^2. \tag{A.5}$$

Assuming some entries of $\mathbf{m}$, $\mathbf{c}$ and/or $\mathbf{k}$ are fixed, this problem takes the form $\min \|\mathbf{Ax}+\mathbf{b}\|_2^2$ subject to $\mathbf{x}\geqslant 0$, that, provided that $\mathbf{A}$ is left-invertible, has a unique solution for the new vector of unknowns $\mathbf{x}$ that contains the free elements of the vectors $\mathbf{m}$, $\mathbf{c}$ and $\mathbf{k}$.

References

[1] B.N. Datta, Finite element model updating, eigenstructure assignment and eigenvalue embedding techniques for vibrating systems, *Mechanical Systems and Signal Processing* 16 (1) (2002) 83–96.

[2] S.W. Doebling, C.R. Farrar, M.B. Prime, A summary review of vibration-based damage identification methods, *The Shock and Vibration Digest* 30 (2) (1998) 91–105.

[3] S.Z. Rad, Methods for Updating Numerical Models in Structural Dynamics, PhD Thesis, University of London, 1997.

[4] R. Kenigsbuch, Y. Halevi, Model updating in structural dynamics: A generalised reference basis approach, *Mechanical Systems and Signal Processing* 12 (1) (1998) 75–90.

[5] K. Alvin, Finite element model update via bayesian estimation and minimization of dynamic residuals, *AIAA Journal* 35 (5) (1997) 879–886.

[6] P. Cha, W. Gu, Model updating using and incomplete set of experimental modes, *Journal of Sound and Vibration* 233 (2000) 587–600.

[7] M. Friswell, D. Inman, D. Pilkey, The direct updating of damping and stiffness matrices, *AIAA Journal* 36 (3) (1998) 491–493.

[8] C. Mares, M. Friswell, J. Mottershead, Model updating using robust estimation, *Mechanical Systems and Signal Processing* 16 (1) (2002) 169–183.

[9] C. Fritzen, D. Jennewein, T. Kiefer, Damage detection based on model updating methods, *Mechanical Systems and Signal Processing* 12 (1) (1998) 163–186.

[10] M.O. Abdalla, K.M. Grigoriadis, D.C. Zimmerman, Enhanced structural damage detection using alternating projection methods, *AIAA Journal* 36 (7) (1998) 1305–1311.

[11] G.-H. Kim, Y.-S. Park, An improved updating parameter selection method and finite element model update using multiobjective optimization technique, *Mechanical Systems and Signal Processing* 18 (1) (2004) 59–78.

[12] M. Baruch, Damage detection based on reduced measurements, *Mechanical Systems and Signal Processing* 12 (1) (1998) 23–46.

[13] Y. Halevi, I. Bucher, Model updating via weighted reference basis with connectivity constraints, *Journal of Sound and Vibration* 265 (2003) 561–581.

[14] S.W. Smith, Iterative matrix approximation for model updating, *Mechanical Systems and Signal Processing* 12 (1) (1998) 187–201.

[15] M. Link, Updating analytical models by using local and global parameters and relaxed optimisation requirements, *Mechanical Systems and Signal Processing* 12 (1) (1998) 7–22.

[16] K. Kwon, R. Lin, Robust finite element model updating using taguchi method, *Journal of Sound and Vibration*, to appear.

[17] B. Datta, S. Elhay, Y. Ram, D. Sarkissian, Partial eigenstructure assignment for the quadratic pencil, *Journal of Sound and Vibration* 230 (1) (2000) 101–110.

[18] S. Kanev, M. Verhaegen, Improved finite element model updating, *First International Operational Modal Analysis Conference (IOMAC)*, Copenhagen, Denmark, 2005.

[19] K.-J. Bathe, *Finite Element Procedures In Engineering Analysis*, Prentice-Hall, Inc., Englewood Cliffs, 1982.

[20] B. Peeters, System Identification and Damage Detection in Civil Engineering, PhD Thesis, Katholieke Universiteit Leuven, 2000, available online via: ⟨http://www.bwk.kuleuven.ac.be/bwm/papers/peet00a.pdf⟩.

[21] Å. Björck, *Numerical Methods for Least Squares Problems*, SIAM, Philadelphia, 1996.

[22] M. Verhaegen, Identification of the deterministic part of MIMO state space models given in innovations form from input–output data, *Automatica* 30 (1) (1994) 61–74.

[23] B. Peeters, G. de Roeck, Reference-based stochastic subspace identification for output-only modal analysis, *Mechanical Systems and Signal Processing* 13 (6) (1999) 855–878.

[24] L. Mevel, L. Hermans, H.V.D. Auweraer, Application of a subspace-based fault detection method to industrial structures, *Mechanical Systems and Signal Processing* 13 (6) (1999) 823–838.

[25] M. Verhaegen, SMI Toolbox, Version 1.0, 2000, Available through ⟨http://www.control.lth.se/∼FRT041/local/index.html⟩.

[26] C. de Boor, *Spline Toolbox User's Guide*, 2004.